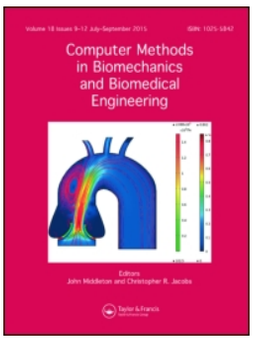

Taylor & Francis
Taylor & Francis Group

Computer Methods in Biomechanics and Biomedical Engineering

ISSN: 1025-5842 (Print) 1476-8259 (Online) Journal homepage: https://www.tandfonline.com/loi/gcmb20

Efficient computational simulation of actin stress fiber remodeling

T. Ristori, C. Obbink-Huizer, C.W.J. Oomens, F.P.T. Baaijens & S. Loerakker

To cite this article: T. Ristori, C. Obbink-Huizer, C.W.J. Oomens, F.P.T. Baaijens & S. Loerakker (2016) Efficient computational simulation of actin stress fiber remodeling, Computer Methods in Biomechanics and Biomedical Engineering, 19:12, 1347-1358, DOI: 10.1080/10255842.2016.1140748

To link to this article: https://doi.org/10.1080/10255842.2016.1140748

Published online: 28 Jan 2016.

COMPUTER METHODS IN BIOMECHANICS AND BIOMEDICAL ENGINEERING, 2016
VOL. 19, NO. 12, 1347–1358
http://dx.doi.org/10.1080/10255842.2016.1140748

Taylor & Francis
Taylor & Francis Group

Efficient computational simulation of actin stress fiber remodeling

T. Ristori[a,b], C. Obbink-Huizer[a], C.W.J. Oomens[a], F.P.T. Baaijens[a,b‡] and S. Loerakker[a,b‡]

[a]Department of Biomedical Engineering, Eindhoven University of Technology, Eindhoven, The Netherlands; [b]Institute for Complex Molecular Systems, Eindhoven University of Technology, Eindhoven, The Netherlands

ABSTRACT

Understanding collagen and stress fiber remodeling is essential for the development of engineered tissues with good functionality. These processes are complex, highly interrelated, and occur over different time scales. As a result, excessive computational costs are required to computationally predict the final organization of these fibers in response to dynamic mechanical conditions. In this study, an analytical approximation of a stress fiber remodeling evolution law was derived. A comparison of the developed technique with the direct numerical integration of the evolution law showed relatively small differences in results, and the proposed method is one to two orders of magnitude faster.

ARTICLE HISTORY
Received 15 June 2015
Accepted 7 January 2016

KEYWORDS
Actin stress fiber remodeling; ODE system with periodic coefficients; analytical approximation; cyclic strain

1. Introduction

The actin stress fiber organization largely influences cell functions and their potential to adapt to their surroundings. These actin bundles are known to be essential for cellular migration (Saez et al. 2007), cellular contractility (Deshpande et al. 2006), and the maturation of other cellular structures such as focal adhesions (Vogel 2006; Johnson et al. 2007). Moreover, they play a crucial role in the remodeling of the extracellular matrix structures, such as collagen. The mechanical properties of soft tissues depend to a large extent on the organization of the collagen network, which is considered as the main load-bearing component in most tissues and the principal contributor to their anisotropic mechanical properties. For example, in heart valves, circumferentially aligned collagen fibers have been observed (Billiar & Sacks 2000a; Martin & Sun 2012) that transfer the pressure applied on the closed heart valve to the aortic wall (Peskin & McQueen 1994). Furthermore, they reinforce the circumferential direction enabling the stretch in the radial direction for a proper closure of the heart valve (Billiar & Sacks 2000a, 2000b; Sacks et al. 2009; Martin & Sun 2012; Fan et al. 2013; Loerakker et al. 2013). Next to external loads (Ruberti & Hallab 2005; Bhole et al. 2009; Wyatt et al. 2009; De Jonge et al. 2013), the collagen network is remodeled by contractile forces exerted by the cells along their principal direction, which is determined by the organization of actin stress fibers (Wang et al. 2003; Ghibaudo et al. 2008; Faust et al. 2011). Therefore, to ensure the functionality of engineered tissues, understanding the process of stress fiber remodeling is necessary.

Like collagen, stress fibers can change their orientation over time. These actin bundles reorient in response to competing stimuli called strain anisotropy, and anisotropy of mechanical resistance (Obbink-Huizer et al. 2014). Experiments have shown that cells orient in the direction perpendicular to the strain when undergoing cyclic strain on a stiff substrate or a biaxially constrained gel (Kaunas et al. 2005; Foolen et al. 2012; Tondon et al. 2012; Foolen et al. 2014). This phenomenon, in response to solely strain anisotropy, is known as strain avoidance and is influenced by the frequency and amplitude of the cyclic strain (Kaunas et al. 2005; Faust et al. 2011; Tondon et al. 2012; Foolen et al. 2014). Anisotropy of mechanical resistance occurs when cells are seeded on a substrate with anisotropic stiffness or residing in a uniaxially constrained gel. In this case, stress fibers remodel in the stiffest direction (Saez et al. 2007; Ghibaudo et al. 2008; Foolen et al. 2012). When a gel is constrained and cyclically strained in the same direction, the effects of strain anisotropy and anisotropy of mechanical resistance are in competition. It has been shown (Foolen et al. 2012; Obbink-Huizer et al. 2014) that the anisotropy of mechanical resistance has often a larger influence in this case, such that cells orient along the constrained direction.

CONTACT S. Loerakker S.Loerakker@tue.nl
‡Baaijens and Loerakker contributed equally.

Several computational models have been proposed to simulate the process of stress fiber remodeling in response to mechanical stimuli (Deshpande et al. 2006; Kaunas & Hsu 2009; Zemel et al. 2010; Vernerey & Farsad 2011; Obbink-Huizer et al. 2014). Deshpande and colleagues developed a computational model that can predict the effects of strain anisotropy and anisotropy of mechanical resistance when separately considered (Deshpande et al. 2006; Wei et al. 2008). Unfortunately, this computational model is inaccurate when the effects of strain anisotropy and anisotropy of mechanical resistance are competing. In 2014, Obbink-Huizer et al. proposed a computational model capable of overcoming these limitations (Obbink-Huizer et al. 2014) by combining two previous models (Deshpande et al. 2006; Vernerey & Farsad 2011).

Recently, Loerakker et al. (2014) have used Obbink-Huizer's computational model to investigate the influence of stress fibers on collagen fiber remodeling when static mechanical stimuli are applied to engineered tissues. The computational simulations were able to predict the collagen organization observed in several experiments. However, the direct numerical integration of the constitutive model for stress fiber development and the calculation of the effects of complex loading profiles on the tissue would lead to excessive computational times in case of dynamic loading conditions. As a result, simulations of soft tissue *in vivo* remodeling in the case of cyclic strain would not be practically feasible.

Obbink-Huizer et al. (2014) have modeled the remodeling process of stress fibers using evolution laws which can be described with a system of ordinary differential equations (ODEs). This system has constant coefficients in case of static mechanical conditions, and periodic coefficients with cyclic loading. While it is possible to determine an analytical solution for constant coefficients, this is not achievable when the coefficients are periodic. In this paper, we provide an analytical approximation for the asymptotic solution of the analyzed system. Furthermore, we propose a strategy to accelerate the computational simulation of stress fiber remodeling. For verification, the simulations presented in the prior study (Obbink-Huizer et al. 2014) have been repeated using the approximation and direct numerical integration. The results show that the developed strategy drastically reduces the computational costs of the integration of the computational model for stress fiber remodeling. Therefore, the new method will enable the simulations of tissue remodeling under cyclic strain. Moreover, the approach can be generalized and applied to other computational simulations involving ODEs with periodic coefficients.

2. Methods

2.1. The computational model proposed by Obbink-Huizer et al. (2014)

Recently, Obbink-Huizer et al. (2014) have published a computational model able to predict the stress fiber distribution in response to the effects of strain avoidance and anisotropy of mechanical resistance. The model was developed considering phenomenological hypotheses for stress fiber remodeling. Briefly, cells were supposed to exert stress onto their surroundings. The value of this stress was a homogenization of the product between the stress fiber stress σ_θ^p, and the stress fiber volume fraction Φ_θ^p over the N considered directions:

$$\boldsymbol{\sigma}^{\text{cell}} = \frac{1}{N}\sum_{\theta} \Phi_\theta^p \sigma_\theta^p \boldsymbol{e}_\theta \boldsymbol{e}_\theta, \tag{1}$$

where $\boldsymbol{e}_\theta$ is the stress fiber orientation in the current state (deformed configuration).

The magnitude of the stress fiber stress along one singular direction was determined with a Hill-type contraction law, dependent on the global Green–Lagrange strain ϵ_θ and strain rate $\dot{\epsilon}_\theta$ in that direction:

$$\sigma_\theta^p = \sigma_{\max} f_\epsilon(\epsilon_\theta) f_{\dot{\epsilon}}(\dot{\epsilon}_\theta), \tag{2}$$

where $\sigma_{\max}$ is the maximal stress fiber stress, while $f_\epsilon(\epsilon_\theta)$ and $f_{\dot{\epsilon}}(\dot{\epsilon}_\theta)$ are functions depending on the strain and strain rate in the direction θ. In particular, $f_{\dot{\epsilon}}$ is a positive increasing function:

$$f_{\dot{\epsilon}}(\dot{\epsilon}_\theta) = \frac{1}{1+\frac{2}{\sqrt{5}}}\left(1 + \frac{k_v\dot{\epsilon}_\theta + 2}{\sqrt{(k_v\dot{\epsilon}_\theta + 2)^2 + 1}}\right), \tag{3}$$

with k_v a positive parameter. f_ϵ is a function composed of an active and a passive part, namely $f_{\epsilon,a}$ and $f_{\epsilon,p}$, which are respectively a gaussian function and a piecewise parabolic function:

$$f_\epsilon = f_{\epsilon,a} + f_{\epsilon,p}; \tag{4}$$

$$f_{\epsilon,a}(\epsilon_\theta) = \exp\left[-\left(\frac{\epsilon_\theta}{\epsilon_0}\right)^2\right]; \tag{5}$$

$$f_{\epsilon,p}(\epsilon_\theta) = \begin{cases} 0 & \text{if } \epsilon_\theta < 0, \\ \left(\dfrac{\epsilon_\theta}{\epsilon_1}\right)^2 & \text{if } \epsilon_\theta \geq 0, \end{cases} \tag{6}$$

where ϵ_0 and ϵ_1 are positive parameters.

Concerning the evolution law for stress fiber remodeling, the depolymerization was supposed to be isotropic, while the synthesis of stress fibers was hypothesized to be dependent on the product between $f_{\epsilon,a}$ and $f_{\dot{\epsilon}}$:

$$\frac{\mathrm{d}\Phi_\theta^p}{\mathrm{d}t} = (k_0^f + k_1^f \sigma_{\max} f_{\epsilon,a} f_{\dot{\epsilon}})\Phi^m - k_d \Phi_\theta^p, \tag{7}$$

where Φ^m is the amount of monomeric actin and k_0^f, k_1^f, and k_d are positive constants. The last equation present in the model is a conservation law of actin mass, which relates Φ^m with the polymerized actin:

$$\Phi^{\mathrm{tot}} = \Phi^m + \frac{1}{N}\sum_\theta \Phi_\theta^p, \tag{8}$$

where Φ^{tot} is a positive constant representing the total actin volume fraction.

With these features, the described computational model was able to predict the stress fiber alignment in numerous experiments, as presented in Obbink-Huizer et al. (2014). However, the resolution of system (7) by means of direct numerical integration requires high computational costs when the stress fibers are subjected to cyclic strain. This limitation has restrained the application of the proposed model for more complex simulations. We propose an analytical approximation for the asymptotic solution of system (7) which will be used to accelerate the computational simulations.

2.2. Approximation for the asymptotic solution of a system of ODEs with periodic coefficients

Consider the following system of ODEs of dimension $n \in \mathbb{N}$

$$\dot{x}(t) = f(t)x(t) + g(t), \tag{9}$$

with $x : \mathbb{R} \to \mathbb{R}^n$ a solution of the system and $f : \mathbb{R} \to \mathbb{R}^{n\times n}, g : \mathbb{R} \to \mathbb{R}^n$ known periodic functions with period $T \in \mathbb{R}^+$ having the following properties:

(I) the asymptotic solution $x_\infty(t)$ of the system is periodic with period T;
(II) either $f(t)$ or $x_\infty(t)$ is almost constant;
(III) $\bar{f} = \frac{1}{T}\int_0^T f(t)\mathrm{d}t$ is an invertible matrix.

In that case, the asymptotic solution can be approximated by

$$\bar{x}_\infty = \frac{1}{T}\int_0^T x_\infty(t)\mathrm{d}t. \tag{10}$$

To approximate $\bar{x}_\infty$, we can substitute $x_\infty(t)$ into Equation (9) and then integrate this equation between 0 and T, dividing by T. Then, the left-hand side of the obtained equation is zero due to the property (I), while on the right-hand side $\frac{1}{T}\int_0^T f(t)x_\infty(t)\mathrm{d}t \approx \bar{f}\bar{x}_\infty$ because of the property (II). At this point, using the property (III), we can obtain:

$$\bar{x}_\infty \approx -\bar{f}^{-1}\bar{g}. \tag{11}$$

2.2.1. Example

As a simple example, consider

$$\dot{x} + x = a + b\cos^2(t), \tag{12}$$

with $x : \mathbb{R} \to \mathbb{R}$ and $a, b \in \mathbb{R}$ constant. In this case our method gives

$$\bar{x}_\infty \approx a + \frac{b}{2}, \tag{13}$$

while the analytical solution is

$$x_\infty(t) = a + \frac{b}{2} + \frac{b}{5}\sin(2t) + \frac{b}{10}\cos(2t). \tag{14}$$

Concluding, our method is able to capture the mean value of the asymptotic solution, while neglecting its oscillations. The oscillations of the asymptotic solution of (7) are expected to be relatively small, so this method seems very suitable for approximating the solution of this system of ODEs.

2.3. Approximation for the asymptotic solution of system (7)

For $N = 1$, when the strain sensed by the stress fibers ϵ_θ is periodic over time with period T (or constant), the asymptotic solution of system (7) tends to a function which has the same period and is slightly oscillating around a constant value (Appendix 1). We assumed this to be true also for higher values of N. We hypothesized that

$$\text{for } t \to +\infty,\ \Phi_\theta^p \to \tilde{\Phi}_\theta^p \text{ for all } \theta, \tag{15}$$

where $\tilde{\Phi}_\theta^p$ are periodic functions with period T and slightly oscillating around constant values. Subsequently, as proposed in the previous section, approximating the asymptotic value of Φ_θ^p was achievable using the mean value of $\tilde{\Phi}_\theta^p$ over its period:

$$\lim_{t\to+\infty}\Phi_\theta^p \approx \frac{1}{T}\int_0^T \tilde{\Phi}_\theta^p \mathrm{d}t. \tag{16}$$

To obtain an analytical expression for this value depending on the profile of the strain, other identities and approximations were necessary. First of all, another identity followed from (15) and the periodicity of $\tilde{\Phi}_\theta^p$:

$$\lim_{t\to+\infty}\int_t^{t+T}\frac{\mathrm{d}\Phi_\theta^p}{\mathrm{d}t}\mathrm{d}t = \int_0^T \frac{\mathrm{d}\tilde{\Phi}_\theta^p}{\mathrm{d}t}\mathrm{d}t = 0. \tag{17}$$

Moreover, using (15) and (16), and observing that $f_{\epsilon,a}$ and $f_{\dot{\epsilon}}$ are periodic in case of periodic strain, the following approximation was possible:

$$\lim_{t\to+\infty}\frac{1}{T}\int_t^{t+T}\left(k_0^f+k_1^f\sigma_{\max}f_{\epsilon,a}f_{\dot{\epsilon}}\right)\Phi_\theta^p\,\mathrm{d}t \approx \frac{1}{T^2}\int_0^T\tilde{\Phi}_\theta^p\,\mathrm{d}t\int_0^T\left(k_0^f+k_1^f\sigma_{\max}f_{\epsilon,a}f_{\dot{\epsilon}}\right)\mathrm{d}t. \quad (18)$$

Finally, an analytical expression for (16) was obtained substituting (8) in (7), integrating the resulting system of ODEs between t and $t+T$ for $t\to+\infty$ using the properties (17) and (18), and solving the subsequent algebraic system with unknown variables $\frac{1}{T}\int_0^T\tilde{\Phi}_\theta^p dt$. As a result, we were able to approximate the asymptotic solution of the system of ODEs (7) with the quantity

$$\lim_{t\to+\infty}\Phi_\theta^p\approx\frac{1}{T}\int_0^T\tilde{\Phi}_\theta^p\,\mathrm{d}t\approx\frac{\bar{a}_\theta}{\sum_\alpha\frac{\bar{a}_\alpha}{N}+k_d}\Phi^{\mathrm{tot}}, \quad (19)$$

where α, the variable in the summation, is covering all the considered stress fiber directions, and

$$\bar{a}_\theta=\frac{1}{T}\int_0^T\left(k_0^f+k_1^f\sigma_{\max}f_{\epsilon,a}(\epsilon_\theta)f_{\dot{\epsilon}}(\dot{\epsilon}_\theta)\right)\mathrm{d}t \quad (20)$$

are auxiliary constants.

2.4. Approach for the computational simulation

Both the direct numerical integration of the ODE system (7), and the application of the dynamic mechanical loads are computationally too expensive to simulate weeks of tissue remodeling. To overcome these limitations, we focused on the asymptotic solution of system (7). The stress fiber remodeling is much faster than the collagen remodeling; thus, to account for the effects of the stress fiber orientation on the collagen remodeling, the final stress fiber configuration is more important than its evolution over time. However, completely eliminating the applied dynamic mechanical loads was not possible. When the deformation changes, the strain profile sensed by the cells is different and this modification influences the system (7). Therefore, knowing how the strains vary over the load cycle is necessary. We included these variations in the stress fiber remodeling algorithm using the coefficients (20) (and consequently (19)). Thus, we reduced the number of applied dynamic mechanical loads to the minimum value necessary to approximate the auxiliary constants defined using (20). For the rest of the remodeling period, the current maximum load was applied.

The following approach was then developed:

- the dynamic mechanical loads were only applied every $M\in\mathbb{N}$ cycles;
- in the remainder of the simulation, the dynamic loads were substituted with a constant mechanical load equal to the current maximum value of the dynamic load, while the dynamic features were used only for the calculation of (20) and subsequently (19);
- the current stress fiber volume fractions were updated assuming that they evolve towards preferred values $\Phi_{\theta,P}^p$ defined using (19) as

$$\Phi_{\theta,P}^p:=\frac{\bar{a}_\theta}{\sum_\alpha\frac{\bar{a}_\alpha}{N}+k_d}\Phi^{\mathrm{tot}}, \quad (21)$$

where the constants $\bar{a}_\theta$ were calculated using (20) at the current configuration, and therefore

$$\frac{\mathrm{d}\Phi_\theta^p}{\mathrm{d}t}=\frac{1}{\tau}\left(\Phi_{\theta,P}^p-\Phi_\theta^p\right) \quad (22)$$

with τ a parameter representing the stress fiber remodeling rate.

2.5. Assessment

To assess the quality of the analytical approximation, the derived computational method was used to simulate the stress fiber remodeling process inside cells residing in three kinds of mechanical environments: having stiffness anisotropy; undergoing cyclic strain with isotropic high stiffness; and again undergoing cyclic strain, but with low stiffness and uniaxially constrained. These simulations were then repeated using the direct numerical integration method used in Obbink-Huizer et al. (2014). Finally, the results and computational times were compared.

Except for the derivation of the solution of system (7) and the application of the dynamic stimuli, the two computational simulation methods were identical; they were performed with the same boundary conditions and material parameters reported in Obbink-Huizer et al. (2014). The main characteristics are reported below.

For the implementation of the material behavior, we used the user subroutine UMAT of the commercial finite element package ABAQUS (Dassault Systèmes Simulia Corp., Providence, RI, USA). A 2D situation was considered in all cases, and cells were supposed to sense the same strain as the substrate. Thus, they were sharing the same mesh of the substrate composed of N_{el} hexahedral elements (C3D8).

Table 1. Parameters for the mechanical models.

Simulation name	3.3 kPa	13 kPa	5 MPa	1a	1b	1c	2a	2b	2c	microtissue
N_{el}	4	4	4	4	4	4	4	4	4	145
E_{NH}	3.3 kPa	13 kPa	5 MPa	1 MPa	1 MPa	1 MPa	1 MPa	1 MPa	1 MPa	10 kPa
E_f	6.6 kPa	26 kPa	10 MPa	–	–	–	–	–	–	–
μ	0.4	0.4	0.4	0.19	0.19	0.19	0.15	0.15	0.15	0.4
f	–	–	–	0.01 Hz	0.1 Hz	1 Hz	0.052 Hz	0.034 Hz	0.009 Hz	0.5 Hz
A	–	–	–	0.1	0.1	0.1	0.049	0.084	0.32	0.1
d	–	–	–	0 s	0 s	0 s	3 s	3 s	3 s	0 s

Parameters taken from Obbink-Huizer et al. (2014).

The substrate was described as a Neo-Hookean compressible material:

$$\boldsymbol{\sigma}^{NH} = \left[\frac{E_{NH}}{3(1-2\nu)}\frac{\ln(J)}{J}\boldsymbol{I} + \frac{E_{NH}}{2(1+\nu)J}(\boldsymbol{F}\boldsymbol{F}^T - J^{2/3}\boldsymbol{I})\right], \tag{23}$$

where $\boldsymbol{\sigma}^{NH}$ is the Cauchy stress in the substrate, $\boldsymbol{F}$ is the deformation tensor with determinant $J = \det(\boldsymbol{F})$, and finally E_{NH} and ν are respectively the Young's modulus and the Poisson's ratio of the substrate. For the simulations of the substrate having anisotropic stiffness, the substrate was reinforced with additional fibers, such that the total substrate stress $\boldsymbol{\sigma}^{\text{sub}}$ was

$$\boldsymbol{\sigma}^{\text{sub}} = \boldsymbol{\sigma}^{NH} + E_f\lambda_f\boldsymbol{e}_f\boldsymbol{e}_f, \tag{24}$$

with E_f the fiber stiffness, λ_f the fiber stretch, and $\boldsymbol{e}_f$ the fiber direction.

The substrate was square-shaped, with a thickness equal to the 10% of the other two dimensions. No stretch was applied to the substrate with anisotropic stiffness, while the loading shape of the dynamic mechanical stimuli present in the other two types of simulations is shown in Figure 1. In addition, symmetry conditions were prescribed in every simulation. The values of the parameters used for the substrate material, and the ones for the stress fiber model are reported in Tables 1 and 2 respectively. The computational simulations were performed assuming that no stress fibers were present at the beginning, and their remodeling was calculated for a time period of $t = 10000$ s. Finally, to take into account the change in density of the discrete fibers in the deformed tissue, the fiber volume fraction in each direction was multiplied by the ratio of the undeformed angle between its two neighboring directions to the corresponding deformed angle (Obbink-Huizer et al. 2014).

Table 2. Parameters for the stress fiber model.

N	20
Φ^{tot}	$5.0e^{-2}$
σ_{max}	$2.0e^{+5}$ Pa
ϵ_0	$1.2e^{-1}$
ϵ_1	$1.7e^{-1}$
k_v	$5.0e^{+1}$ s
k_0^f	$1.5e^{-6}$ s^{-1}
k_1^f	$7.00e^{-7}$ s^{-1}Pa^{-1}
k_d	$1.00e^{-3}$ s^{-1}

Parameters taken from Obbink-Huizer et al. (2014).

3. Results

3.1. Anisotropic substrate

Experimental studies have demonstrated that cells on anisotropic substrates orient along the stiffest direction (Saez et al. 2007; Ghibaudo et al. 2008). This alignment is more evident with decreasing absolute stiffness. The computational model of Obbink-Huizer et al. (2014) is able to capture these characteristics. As shown in Figure 2, the analytical approximation perfectly replicated the results obtained using direct numerical integration. This result is particularly evident in the bottom graphs of Figure 2, which shows that the results are equal in all fiber directions.

3.2. Cyclic strain applied to a high stiffness substrate

On a high stiffness substrate subjected to a cyclic strain of various amplitudes and frequencies, stress fibers remodel to avoid the strain and align perpendicular to the direction of cyclic strain (Kaunas et al. 2005; Tondon et al. 2012). Figure 3 compares the results of the simulations of this phenomenon. For every case, the analytical approximation gave predictions very similar to the direct numerical integration. For low frequencies (Figure 3(1a) and (1b)) and low amplitudes (Figure 3(2a) and (2b)), the predicted stress fibers distributions were approximately the same. Larger differences were visible with increasing frequency (Figure 3(1c)) or amplitude (Figure 3(2c)). Nevertheless, even when the differences were quantitatively larger (Figure 3, bottom), the results were still qualitatively similar.

3.3. Cyclic strain applied to a low stiffness environment

Finally, cells embedded in a uniaxially constrained collagen gel exposed to cyclic strain were simulated. In the experiments, despite the cyclic strain, the stress fibers

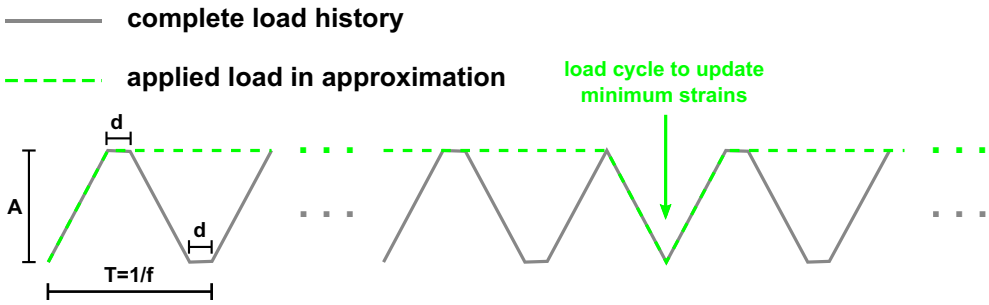

Figure 1. Cyclic loading profile, adapted from Obbink-Huizer et al. (2014).

aligned parallel to the direction of this mechanical stimulus (Foolen et al. 2012; Obbink-Huizer et al. 2014). In addition to the equilibrium stress fiber distribution, the deformation of the tissue resulting from the two simulations was obtained. As can be seen from Figure 4, the deformed configurations were very similar. Concerning the stress fiber volume fractions, compared to the previous simulations (Figures 2 and 3), larger dissimilarities were visible between the two methods (Figure 5, bottom). However, the main orientation of the actin stress fibers was successfully estimated for every location using the analytical approximation (Figure 5, top and center).

3.4. Comparison of the computational times

As illustrated in Figure 6, the analytical approximation was computationally less expensive for every simulation. The computational time necessary to run the simulations with direct numerical integration strongly increased when increasing the frequency or amplitude of the applied cyclic strain. Interestingly, using the analytical approximation, this behavior was no longer observed; the computational time remained almost constant when the frequency and amplitude of the stretch were changed. As a result, as can be seen observing Figure 7, the proposed strategy was particularly more efficient in case of large amplitudes and frequencies of strain, as well as complex deformations. For instance, the microtissue simulation took slightly less than 19 h with the direct numerical integration scheme (67960 s), and only 256 s using the approach with the analytical approximation.

4. Discussion

The purpose of this study was to develop an approach to efficiently predict actin stress fiber remodeling by means of computational simulations. The model proposed by Obbink-Huizer et al. (2014) is able to predict the stress fiber alignment for a range of experimental conditions. Thus, we chose to analyze this computational model and to determine a method to accelerate the related computational simulations. The asymptotic solution of the ODE system which describes the stress fiber evolution was analytically approximated. Then, an approach to benefit from this approximation was derived, such that the final outcome of the simulations can be obtained without applying the complete dynamic deformation profile over time.

To assess the quality of the proposed approach, the same computational simulations reported in Obbink-Huizer et al. (2014) were performed using direct numerical integration and the analytical approximation. Then, the results and computational times were compared. In particular, actin stress fiber remodeling was simulated for cells seeded on an anisotropic substrate and on a uniaxially stretched isotropic substrate, and then for cells embedded in a gel uniaxially constrained and stretched.

The main predicted SF alignment was similar when the analytical approximation was used instead of direct numerical integration. In particular, the results of the two methods were identical when simulations of tissue remodeling under static conditions were performed (Figure 2). An explanation for this is that, in the absence of dynamic mechanical stimuli, the system (7) has constant coefficients and, as a consequence, the approximation (19) becomes the exact solution. Conversely, the outcomes differed slightly when cyclic strain was applied to the tissue. In particular, the dissimilarities increased when increasing the strain frequency, strain amplitude, or decreasing the stiffness (Figures 3 and 5). All these changes involve larger deformations, so this phenomenon underlines a correlation between the deformation of the tissue and the quality of the approximation; more deformation corresponds to larger differences between the results obtained using direct numerical integration and the analytical approximation. These discrepancies may be due to a propagation of approximations. On the one hand, the constants $\bar{a}_\theta$ used to compute the preferred value $\Phi^p_{\theta,P}$ (respectively defined in (20) and (21)) were calculated by means of the profile of the strain sensed by the cells, which was obtained using

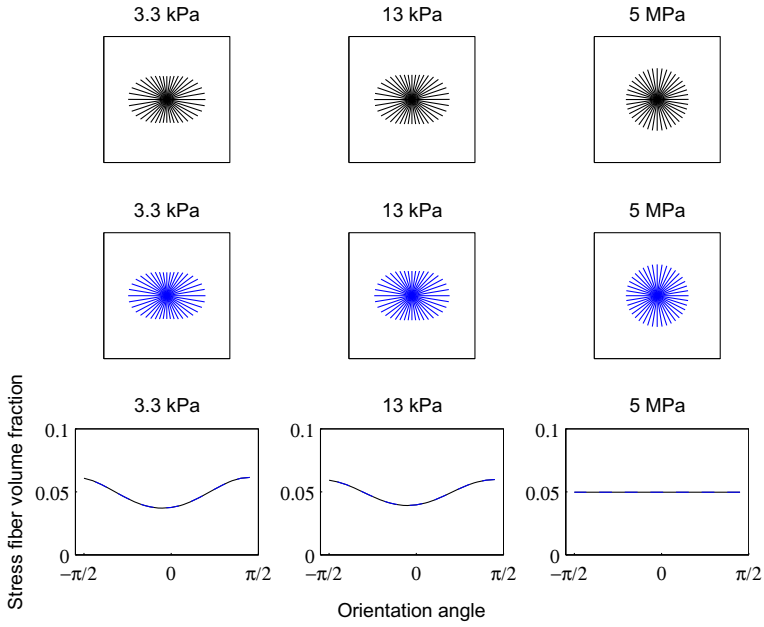

Figure 2. Stress fiber distribution for cells cultured on a substrate with varying values of substrate and horizontal reinforcing fiber stiffness (E_{NH} and E_f respectively). On top of each figure, there are the values of E_{NH}, while $E_f = 2E_{NH}$ in every case. The results are obtained using direct numerical integration (top, and black on the bottom) and the analytical approximation (center, and blue on the bottom). In the top and central figures, the length of the lines in each direction is proportional to the associated stress fiber volume fraction.

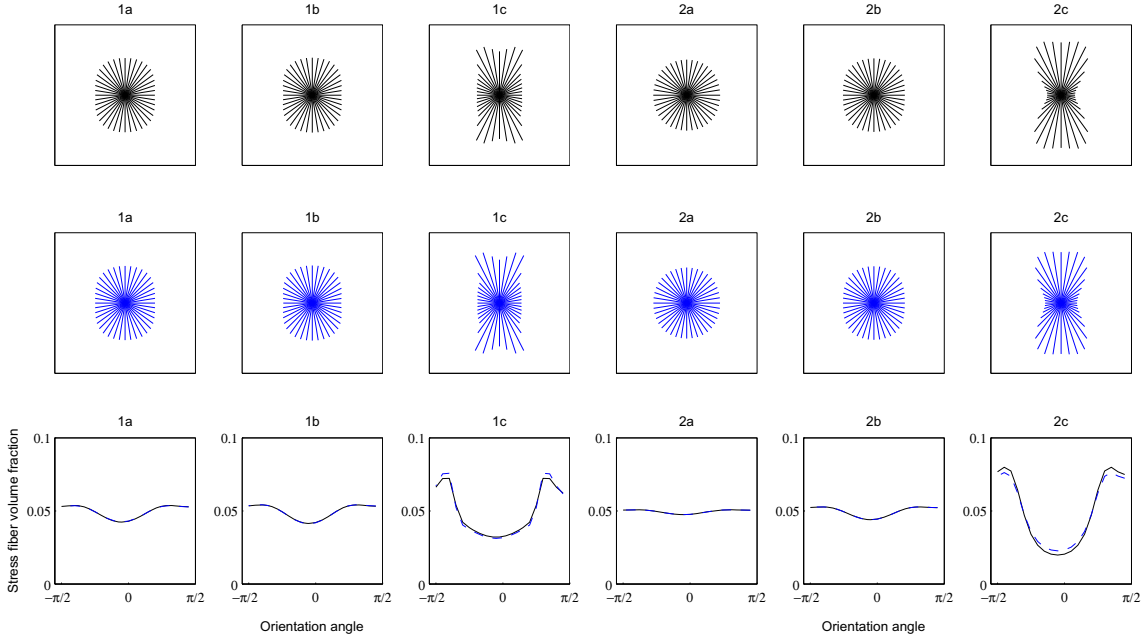

Figure 3. Stress fiber distribution for cells cultured on a high stiffness substrate cyclically strained using several frequencies and amplitudes (Table 1). The direction of the strain is horizontal. The results were obtained using direct numerical integration (top, and black on the bottom) and the analytical approximation (center, and blue on the bottom). In the top and central figures, the length of the lines in each direction is proportional to the associated stress fiber volume fraction.

the deformation. On the other hand, the deformations depended on the stress fiber stress which was influenced by the stress fiber organization and, therefore, by the constants $\bar{a}_\theta$.

In conclusion, as expected, the proposed method does not provide a perfect solution of the ODE system (7), but an approximation. However, the discrepancies between the two computational approaches are much smaller than the experimentally observed variations (Saez et al. 2007; Ghibaudo et al. 2008; Kaunas & Hsu 2009; Foolen et al. 2012). Consequently, the inaccuracy of the herein proposed method is acceptable.

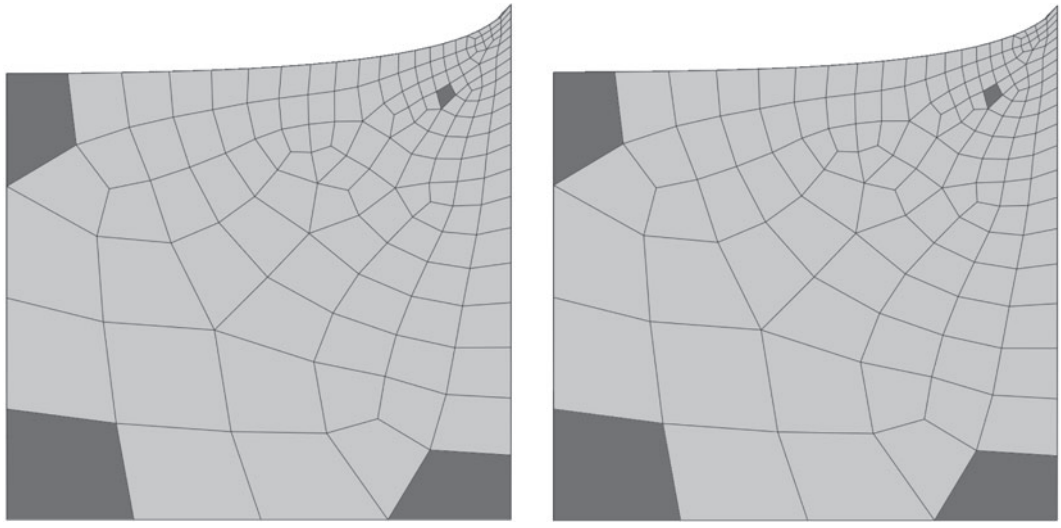

(a) Direct numerical integration. (b) Analytical approximation.

Figure 4. Equilibrium configuration of the deformed tissue resulting from the simulations of cells embedded in an environment with low stiffness, cyclically strained in the horizontal direction at an amplitude of 10% and a frequency of 0.5 Hz. The black color highlights the elements chosen to compare the local stress fiber distributions shown in Figure 5.

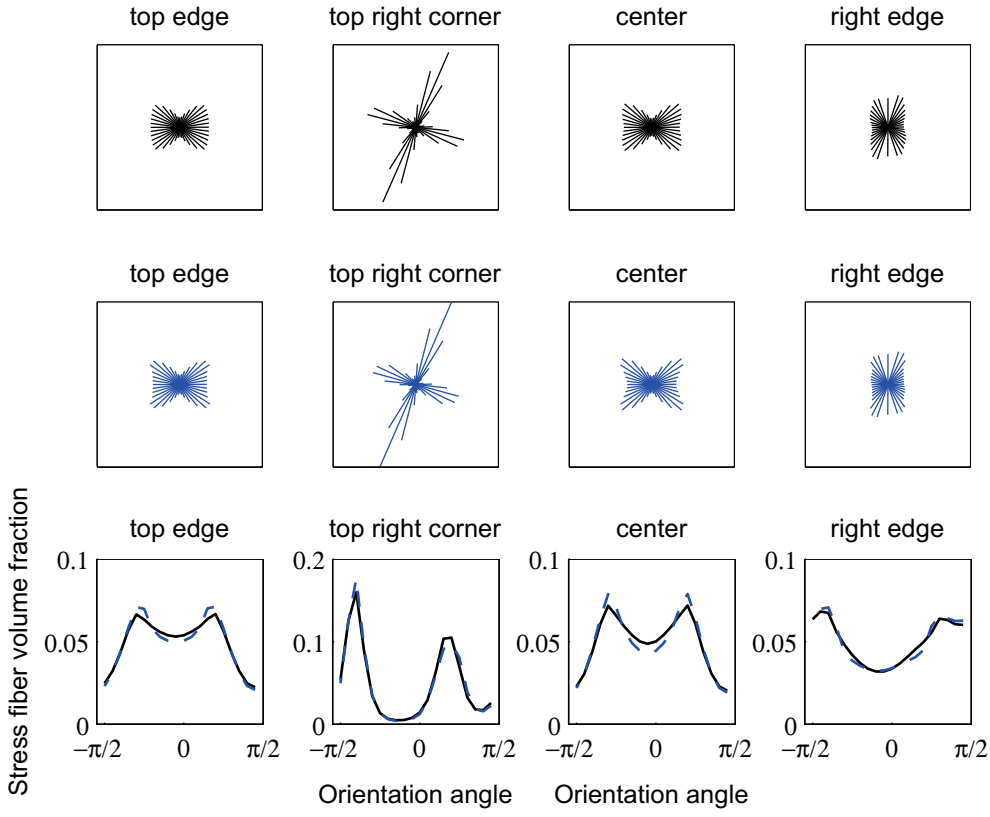

Figure 5. Stress fibers distribution for cells cultured on a low stiffness substrate cyclically strained at an amplitude of 10% and a frequency of 0.5 Hz. The direction of the strain is horizontal. The results were obtained using direct numerical integration (top, and black on the bottom) and the analytical approximation (center, and blue on the bottom). In the top and central figures, the length of the lines in each direction is proportional to the associated stress fiber volume fraction.

Most importantly, for every simulation the proposed approach is faster than the direct numerical integration. Interestingly, as shown in Figure 7, larger dissimilarities between the two computational algorithms correspond to larger advantages in terms of computational times. Figure 6 suggests that this phenomenon may be again related to the deformation magnitudes. Larger deformations lead to increased computational costs. Our

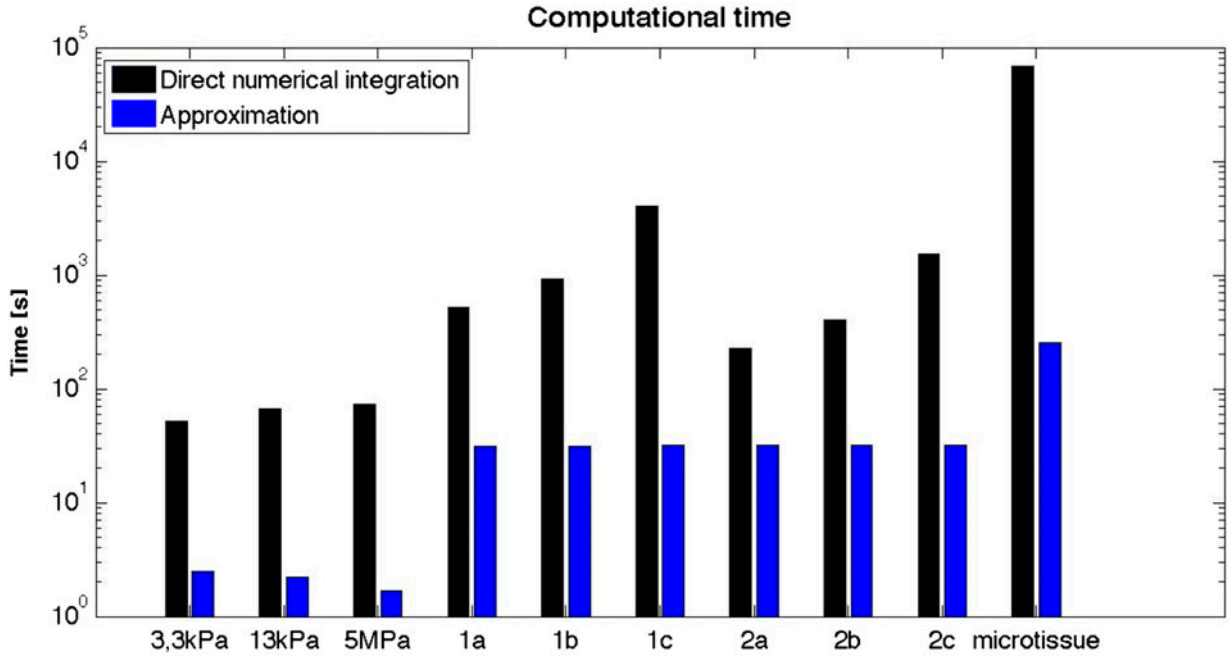

Figure 6. Comparison of the computational times necessary for the simulations.

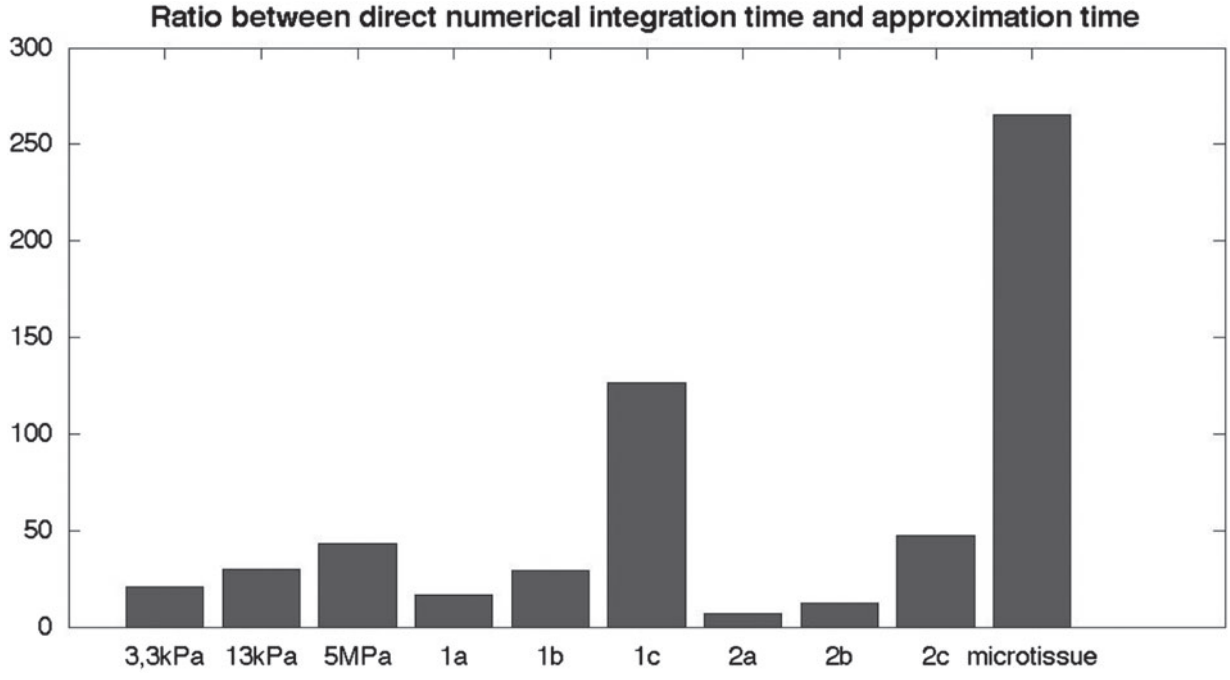

Figure 7. Comparison of the computational times necessary for the simulations.

approach was relatively unaffected by this process because we used a small number of loading cycles. This explanation is supported by the results shown in Figure 6. In fact, for the simulations of cells seeded on a uniaxially stretched isotropic substrate, the computational time varied with the frequency and amplitude of the strain when direct numerical integration was used, while it was constant for the analytical approximation. Therefore, our approach overcomes the limitations related to the application of the dynamic mechanical stimuli, even if the inclusion of some loading cycles was still needed due to the calculations of the auxiliary constants $\bar{a}_\theta$.

The proposed strategy can be generalized and inserted into the context of numerical methods for the resolution of ODEs that have solutions with high frequencies (Petzold 1981; Petzold et al. 1997; Hairer et al. 2006). However, while these numerical methods are able to cap-

ture the slow oscillations of the solutions and neglect the fast oscillations, our method approximates the average value of the solutions and neglects all the oscillations. Therefore, it is suitable to solve problems only when a slightly constant solution is expected. This is the case for ODEs describing the process of SF remodeling, as these fibers are expected to reach a homeostatic configuration. Concerning the point of view of computational efficiency, further numerical analysis is necessary to compare the proposed strategy to other numerical methods. Regarding the analytical approximation, a similar approach was previously used by Wei et al. (2008) to approximate the computational model of Deshpande et al. (2006) for stress fiber remodeling. However, this approximation was applied only to a single ODE and not generalized for a system of ODEs. Furthermore, in our study, the approximation led to the development of a subsequent numerical method suitable for finite element simulations where the profiles of strain and strain rate can slightly vary over time.

In summary, the previously shown results demonstrate that the new approach provides efficient computational simulations of stress fiber remodeling. This result may have major consequences for future research on predicting tissue remodeling. In fact, not only are these findings advantageous for stress fiber remodeling simulations, but they also open to the possibility to computationally investigate the long term effects of collagen remodeling on soft tissues and to include the effects of dynamic loading conditions. Moreover, the numerical method derived in this research can be generalized, and it is applicable to other ODE systems of first order with periodic coefficients.

Disclosure statement

No potential conflict of interest was reported by the authors.

Funding

This work was supported by the People Programme (Marie Curie Actions) of the European Union's Seventh Framework Programme [FP7/2007-2013/]; REA [grant agreement number 317512].

References

Bhole AP, Flynn BP, Liles M, Saeidi N, Dimarzio CA, Ruberti JW. 2009. Mechanical strain enhances survivability of collagen micronetworks in the presence of collagenase: implications for load-bearing matrix growth and stability. Philos Trans A Math Phys Eng Sci. 376:3339–3362.

Billiar KL, Sacks MS. 2000a. Biaxial mechanical properties of the natural and glutaraldehyde-treated aortic valve cusp-part I: experimental results. J Biomech Eng. 122:23–30.

Billiar KL, Sacks MS. 2000b. Biaxial mechanical properties of the natural and glutaraldehyde-treated aortic valve cusp-part II: a structural constitutive model. J Biomech Eng. 122:327–335.

De Jonge N, Kanters FMW, Baaijens FPT, Bouten CVC. 2013. Strain-induced collagen organization at the micro-level in fibrin-based engineered tissue constructs. Ann Biomed Eng. 41:763–774.

Deshpande VS, McMeeking RM, Evans AG. 2006. A bio-chemo-mechanical model for cell contractility. Proc Natl Acad Sci USA. 103:14015–14020.

Fan R, Bayoumi AS, Chen P, Hobson CM, Wagner WR, Mayer JE, Jr., Sacks MS. 2013. Optimal elastomeric scaffold leaflet shape for pulmonary heart valve leaflet replacement. J Biomech. 46:662–669.

Faust U, Hampe N, Rubner W, Kirchgessner N, Safran S, Hoffmann B, Merkel R. 2011. Cyclic stress at mHz frequencies aligns fibroblasts in direction of zero strain. Plos One 6:e28963.

Foolen J, Deshpande VS, Kanters FMW, Baaijens FPT. 2012. The influence of matrix integrity on stress-fiber remodeling in 3D. Biomaterials. 33:7508–7518.

Foolen J, Janssen-van den Broek MWJT, Baaijens FPT. 2014. Synergy between Rho signaling and matrix density in cyclic stretch-induced stress fiber organization. Acta Biomater. 10:1876–85.

Ghibaudo M, Saez A, Trichet L, Xayaphoummine A, Browaeys J, Silberzan P, Buguinb A, Ladoux B. 2008. Traction forces and rigidity sensing regulate cell functions. Soft Matter. 4:1836–1843.

Hairer E, Wanner G, Lubich C. 2006. Geometric numerical integration. Structure-preserving algorithms for ordinary differential equations. Springer Series in Computational Mathematics. 2nd ed. 31, Springer-Verlag: Berlin; p. xviii–644.

Kaunas R, Nguyen P, Usami S, Chien S. 2005. Cooperative effects of Rho and mechanical stretch on stress fiber organization. Proc Natl Acad Sci USA 102:15895–15900.

Kaunas R, Hsu HJ. 2009. A kinematic model of stretch-induced stress fiber turnover and reorientation. J Theor Biol. 257:320–330.

Johnson CP, Tang H-Y, Carag C, Speicher DW, Discher DE. 2007. Forced unfolding of proteins within cells. Science. 317:663–666.

Loerakker S, Argento G, Oomens CWJ, Baaijens FPT. 2013. Effects of valve geometry and tissue anisotropy on the radial stretch and coaptation area of tissue-engineered heart valves. J Biomech. 46:1792–1800.

Loerakker S, Obbink-Huizer C, Baaijens FPT. 2014. A physically motivated constitutive model for cell-mediated compaction and collagen remodeling in soft tissues. Biomech Model Mechanobiol. 13:985–1001.

Martin C, Sun W. 2012. Biomechanical characterization of aortic valve tissue in humans and common animal models. J Biomed Mater Res A. 100:1591–1599.

Obbink-Huizer C, Oomens CWJ, Loerakker S, Foolen J, Bouten CVC, Baaijens FPT. 2014. Computational model predicts cell orientation in response to a range of mechanical stimuli. Biomech Model Mechanobiol. 13:227–236.

Peskin CS, McQueen DM. 1994. Mechanical equilibrium determines the fractal fiber architecture of aortic heart valve leaflets. Am J Physiol. 266:H319–28.

Petzold LR. 1981. An efficient numerical method for highly oscillatory ordinary differential equations. SIAM J Numer Anal. 18:455–479.
Petzold LR, Jay LO, Yen J. 1997. Numerical solution of highly oscillatory ordinary differential equations. Acta Numerica. 6:437–483.
Ruberti JW, Hallab NJ. 2005. Strain-controlled enzymatic cleavage of collagen in loaded matrix. Biochem Biophys Res Commun. 336:483–489.
Sacks MS, David Merryman W, Schmidt DE. 2009. On the biomechanics of heart valve function. J Biomech. 42:1804–1824.
Saez A, Ghibaudo M, Buguin A, Silberzan P, Ladoux B. 2007. Rigidity-driven growth and migration of epithelial cells on microstructured anisotropic substrates. Proc Natl Acad Sci USA. 20:8281–8286.
Tondon A, Hsu HJ, Kaunas R. 2012. Dependence of cyclic stretch-induced stress fiber reorientation on stretch waveform. J Biomech. 45:728–35.
Vernerey FJ, Farsad M. 2011. A constrained mixture approach to mechano-sensing and force generation in contractile cells. J Mech Behav Biomed Mater. 4:1683–99.
Vogel V. 2006. Mechanotransduction involving multimodular proteins: converting force into biochemical signals. Annu Rev Byophys Biomol Struct. 35:459–488.
Wang JHC, Jia F, Gilbert TW, Woo SLY. 2003. Cell orientation determines the alignment of cell-produced collagenous matrix. J Biomech. 36:97–102.
Wei Z, Deshpande VS, McMeeking RM, Evans AG. 2008. Analysis and interpretation of stress fiber organization in cells subject to cyclic stretch. J Biomech Eng. 130:031009.
Wyatt KEK, Bourne JW, Torzilli PA. 2009. Deformation-dependent enzyme mechanokinetic cleavage of type I collagen. J Biomech Eng. 131:051004.
Zemel A, Rehfeldt F, Brown AEX, Discher DE, Safran SA. 2010. Optimal matrix rigidity for stress fiber polarization in stem cells. Nat Phys. 6:468–473.

Appendix 1. Analytical analysis of system (7) for $N = 1$

In this paper, we approximated the asymptotic solution of the ODE system (7) which was introduced in Obbink-Huizer et al. (2014) to describe the stress fiber remodeling process. In particular, the analytical approximation was obtained assuming that the asymptotic behavior of the solution in case of a periodic strain is periodic and slightly oscillating around a constant value. The assumption can be explained through an analysis of the ODE system (7) for $N = 1$. When only one direction for the stress fibers is considered, defining the solely unknown variable as Φ and substituting (8) into (7), the ODE system becomes

$$\dot{\Phi} + (a + k_d)\Phi = a\Phi^{\text{tot}}, \tag{A1}$$

where a is an auxiliary function dependent on the deformation profile and defined as

$$\begin{aligned} a &:= k_0^f + k_1^f \sigma_{\max} f_{\epsilon,a}(\epsilon) f_{\dot{\epsilon}}(\dot{\epsilon}) \\ &= k_0^f + \frac{k_1^f \sigma_{\max}}{1 + 2/\sqrt{5}} \left(1 + \frac{k_v \dot{\epsilon} + 2}{\sqrt{(k_v \dot{\epsilon} + 2)^2 + 1}}\right) \exp\left(-(\epsilon/\epsilon_0)^2\right). \end{aligned} \tag{A2}$$

The Equation (A1) is an ordinary differential equation with coefficients dependent on the strain profile, and it has the analytical solution

$$\Phi(t) = \exp\left(-A(t)\right)\left[\Phi^{\text{tot}} \int_0^t \exp\left(A(\tau)\right) a(\tau) d\tau + \Phi(0)\right], \tag{A3}$$

where A is the following auxiliary function:

$$A(t) = \int_0^t (a(\tau) + k_d) d\tau. \tag{A4}$$

The integrand of the function $A(t)$ is strictly positive for every value of t, thus

$$\lim_{t \to +\infty} \exp\left(-A(t)\right) = 0. \tag{A5}$$

As a consequence, the asymptotic behavior of the solution of the ODE (A1) corresponds to the function

$$\tilde{\Phi}(t) := \Phi^{\text{tot}} \exp\left(-A(t)\right)\psi(t), \tag{A6}$$

where

$$\psi(t) = \int_0^t \exp\left(A(\tau)\right) a(\tau) d\tau. \tag{A7}$$

So far, we did not use the periodicity of the applied strain. In what follows, a representation for the function $\tilde{\Phi}(t)$ which benefits from the properties of the periodic strain will be derived. First of all, if we suppose that $\epsilon(t)$ is a periodic function of period T, then also a has the same characteristics. In fact,

$$\begin{aligned} a(t+T) &= k_0^f + \frac{k_1^f \sigma_{\max}}{1 + 2/\sqrt{5}} \left(1 + \frac{k_v \dot{\epsilon}(t+T) + 2}{\sqrt{(k_v \dot{\epsilon}(t+T) + 2)^2 + 1}}\right) \\ &\quad \times \exp\left(-(\epsilon(t+T)/\epsilon_0)^2\right) \end{aligned} \tag{A8}$$

$$\begin{aligned} &= k_0^f + \frac{k_1^f \sigma_{\max}}{1 + 2/\sqrt{5}} \left(1 + \frac{k_v \dot{\epsilon}(t) + 2}{\sqrt{(k_v \dot{\epsilon}(t) + 2)^2 + 1}}\right) \\ &\quad \times \exp\left(-(\epsilon(t)/\epsilon_0)^2\right) = a(t). \end{aligned} \tag{A9}$$

Concerning A, proving that

$$A(t+T) = A(t) + k_d T + \int_0^T a(\tau) \mathrm{d}\tau \tag{A10}$$

is possible using algebraic properties of the integrals and the periodicity of a. As a consequence, the following identity can be derived:

$$\exp[A(t+jT)] = \exp[A(t)] d^j \quad \forall j \in \mathbb{Z}, \tag{A11}$$

where d is a constant defined with $d = \exp\left(k_d T + \int_0^T a(\tau) \mathrm{d}\tau\right)$.

The last term of the function $\tilde{\Phi}(t)$ that has to be analyzed is $\psi(t)$. Using the periodicity of a, Equation (A11), and algebraic passages, the function $\psi(t)$ can be rewritten as

$$\psi(t) = \psi(T) \sum_{j=0}^{\lfloor \frac{t}{T} \rfloor - 1} d^j + d^{\lfloor \frac{t}{T} \rfloor} \psi\left(t - \left\lfloor \frac{t}{T} \right\rfloor T\right). \tag{A12}$$

Substituting (A11) and (A12) in Equation (A6), a representation for $\tilde{\Phi}(t)$ can be found:

$$\tilde{\Phi}(t) = \Phi^{\text{tot}} \exp\left(-A\left(t - \left\lfloor \frac{t}{T} \right\rfloor T\right)\right) \times \left(\psi(T) \sum_{j=1}^{\left\lfloor \frac{t}{T} \right\rfloor} d^{-j} + \psi(t - \left\lfloor \frac{t}{T} \right\rfloor T)\right), \tag{A13}$$

where $\psi(t) := \int_0^t a(\tau) \exp(A(\tau)) \mathrm{d}\tau$. The last representation can be derived noting that

$$\lim_{t \to +\infty} \sum_{j=1}^{\left\lfloor \frac{t}{T} \right\rfloor} d^{-j} = \frac{1}{d-1}. \tag{A14}$$

Concluding, we have derived a new representation for the function $\tilde{\Phi}(t)$ which describes the behavior of the solution of (A1):

$$\tilde{\Phi}(t) = \Phi^{\text{tot}} \exp\left(-A\left(t - \left\lfloor \frac{t}{T} \right\rfloor T\right)\right) \times \left(\frac{\psi(T)}{d-1} + \psi\left(t - \left\lfloor \frac{t}{T} \right\rfloor T\right)\right). \tag{A15}$$

Proving that the asymptotic solution of (A1) is periodic is then possible using Equation (A15), and noting that $t - \left\lfloor \frac{t}{T} \right\rfloor T = t + T - \left\lfloor \frac{t+T}{T} \right\rfloor T$.

$\tilde{\Phi}(t)$ is also slightly oscillating around a constant value. In fact, it is composed of a constant term $\frac{\psi(T)}{d-1}$ which is added to an increasing function and multiplied with a decreasing function.